ADVANCED FUNCTIONAL MATERIALS

FULL PAPER

DOI: 10.1002/adfm.200701431

Quantitative analysis of lattice ordering in thin film opal-based photonic crystals**

By *Worawut Khunsin, Gudrun Kocher, Sergei G. Romanov,** and *Clivia M. Sotomayor Torres*

This work is devoted to the quantitative evaluation of the lattice ordering of opal films. Assembling colloidal crystals in a moving meniscus under random noise agitation produced opal films with generically the same lattice but different disorders. The lattice ordering is quantified by the magnitudes of harmonics in the Fourier transforms of (i) the scanning electron microscopy images to address the in-plane lattice ordering and (ii) rotation diagrams of the optical transmission to address the regularity of crystal planes. In prepared opals, the strong deviation of the lattice from the face-centered cubic symmetry is demonstrated. We find uneven lattice responses to changing the growth conditions, e.g., the 30% improvement of the hexagonal lattice ordering in the (111) growth plane accompanied by a ten-time better ordering of (220) planes as a result of noise agitation. The suggested approach to characterize crystalline quality of the lattice is a general methodology that can be applied to the analysis of other three-dimensional photonic crystals.

1. Introduction

Photonic crystals (PhCs) are periodic structures for manipulating the propagation and emission of light.[1] Many functionalities, like waveguiding,[2] lasing,[3] filtering,[4] and routing have been explored in one-, two-, and three-dimensional (3-D) PhCs, over a broad portion of electromagnetic spectrum from microwaves to near-UV regions.[5–8] 3-D PhCs are of particular interest since they are capable of full control upon the light propagation in the case of omnidirectional photonic bandgap.[9] However, the complexity of fabrication of PhCs increases with increasing their dimensionality including the cost,[10] alignment,[11,12] and time [13,14] issues. In this context, self-assembly of colloidal crystals is a low-cost alternative to other nanofabrication methods.[15] The resulting structures, opals, are 3-D lattices of spherical particles converging towards the face-centered cubic (fcc) symmetry.[16] However, opal crystals are susceptible to large scale lattice distortions, e.g., stacking faults[17] and the lattice twinning,[18,19] due to the small difference in the free energy between fcc and hexagonal close packed (hcp) lattices.

In the past decade, a number of methods were proposed to improve the crystalline quality of opals. This includes, for example, the self-assembly under controlled air flux,[20] temperature,[21] and humidity,[22] the crystallization in confined cells,[23] and on non-wetting substrates.[24] In general, the growth conditions are such that the spheres organize themselves by a combination of Brownian motion, multiple-particle interaction and electrostatic forces into the most thermodynamically favorable fcc crystal lattice.[16] However, the substrate acts as an anchorage point for the spheres that freezes their instant lattice configuration and conserves the stressed lattice.[18] To relax this limitation the spheres should remain mobile up to the last stage of drying. This limitation is particularly severe in the case of the crystallization in a vertically moving meniscus, because the crystallization time is much shorter than that in sedimented opals. A number of proposals have been made to optimize the motion of spheres at the meniscus so as to recreate the near-equilibrium condition leading to a larger fraction of spheres occupying the positions with the fcc arrangement.[20–22] Despite impressive improvements in local arrangements,[25–28] judged from scanning electron microscope (SEM) images, limited efforts have been made to provide a quantitative evaluation of the long-range regularity of the opal lattice, neither of spheres within the plane nor the planes in the lattice.

To facilitate a quantitative comparison between opals films with different lattice ordering, we studied opals crystallized in

[*] Dr. S. G. Romanov, Dr. G. Kocher, W. Khunsin, Prof. C. M. Sotomayor Torres
Tyndall National Institute
University College Cork, Lee Maltings, Cork (Ireland)
E-mail: sergei.romanov@tyndall.ie
Dr. S. G. Romanov
Ioffe Physical Technical Institute, 194021,
Polytekhnicheskaya ul., 26, St. Petersburg (Russia)
Prof. C. M. Sotomayor Torres
Catalan Institute for Research and Advanced Studies
ICREA, 08010 Barcelona (Spain)
Prof. C. M. Sotomayor Torres
Catalan Institute of Nanotechnology, Edifici CM7
Campus Universitat Autonoma de Barcelona, 08193 Bellaterra (Spain)

[**] This material is based upon work supported in part by the Science Foundation Ireland Grant No. 02/IN.1/172, the EU IST projects "PHAT" and the NoE PhOREMOST, and the RFBR Grant No. 05-02-16975-a. The authors would like to thank Prof. R. Zentel at the University of Mainz (Germany) for the gift of the PMMA suspension.

an acoustic white noise field. Acoustic vibrations increases effectively the crystallization time in the meniscus leading to the formation of less stressed lattice, without changing the generic symmetry of the lattice. Hence, in this work we compared the ordering in lattices crystallized in more and less equilibrium conditions in contrast to previous studies that were carried out on ordering degradation.[29]

Although direct information about opal lattice ordering can be obtained using the low-angle neutron[30] and X-ray scattering,[31] these methods are not commonly used. In general, optical methods are more convenient. Lattice symmetry can be revealed in the study of diffraction patterns using tunable laser when a sufficiently small refractive index contrast and special observation conditions to visualize high-order diffraction are met.[32] Alternatively, the optical quality of the material can naturally be estimated in terms of the photon mean free path,[33] but this approach is difficult to link to a particular lattice configuration. The most straightforward way of estimating the lattice ordering is by fitting the numerically simulated transmission spectra with experimental data by introducing all relevant defects into a numerical model. However, this method requires *a priori* knowledge of defects and is intrinsically time and resource consuming at present.

In this paper, we describe two other approaches to the evaluation of the regularity of crystal lattice in thin opal films based on the Fourier transform (FT) analysis. It is straightforward to apply the FT to the SEM images of the 2-D lattice of spheres in the growth (111) plane in order to quantitatively evaluate its ordering, but no quantitative comparison of different lattices has been reported to date. More complicated task is to apply the FT analysis to optical diffraction spectra to visualize the ordering of different planes in a 3-D lattice. To achieve this, we presented the optical transmission as a function of the rotation angle around the normal to the growth plane, namely, the [111] axis. Applying FT analysis to the transmission patterns of planes with the same crystallographic indices allows the evaluation of the axial symmetry in the lattice. The assignment of the transmission minima to particular planes was made by tracing the dispersion of the minima obtained at different incidence angles. The applied analysis allowed us to compare the actual symmetry of opal crystals with that of the fcc lattice and to reveal the crystal planes, which are most susceptible to lattice disorder.

2. Experimental Technique

Samples were prepared in a vertically moving meniscus from polymethylmetacrylate (PMMA) spheres with a diameter $D = 368$ nm on a glass substrate. In order to improve crystal ordering, an acoustic field with low frequency white noise spectrum was used to add chaotic displacement to the suspension of colloidal particles thereby enhancing force equilibrium during opal crystallization (Fig. 1a). Detailed description of this technique is given elsewhere.[34] In what follows we will refer to the opal film crystallized without acoustic agitation as sample A and the film crystallized in the acoustic noise field as sample B.

Angle-resolved transmission measurements were used to characterize light diffraction in a 3-D crystal. Figure 1b schematically depicts the measurement configuration. In the first instance, the diffraction was studied as a function of the angle of the light beam incidence, θ, with respect to the [111] axis of the fcc lattice. Scanning the angle of incidence was performed for three different orientations of the plane of incidence with respect to the lattice that is equivalent to tracing the transmission along three non-equivalent high symmetry orientations, LKL', LUX, and LW, in the Brillouin zone of the fcc lattice. This allows us to assess the diffraction from planes of different crystallographic indices. Secondly, the plane of incidence was rotated around the [111] axis by changing the azimuth angle, φ, for a fixed angle of incidence to obtain the azimuth variation of the transmission. The inset to Figure 1b shows the unfolded view of the first Brillouin zone of the fcc lattice, where the dotted line along the $L'KLUX$ orientation lies in the incident plane (θ, $\varphi = 0°$) and the dashed circle represents the trace of incident light beam for azimuth measurement: ($\theta = 65°$, φ).

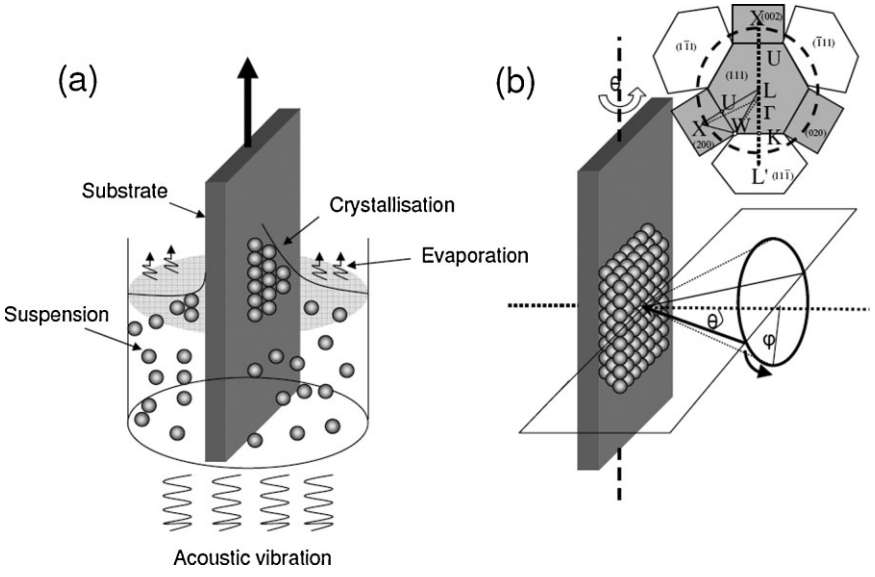

Figure 1. a) Schematics of the opal crystallization set-up. The spheres are crystallized on a vertically oriented glass substrate, which is drawn out of the suspension by a stepper motor. The acoustic agitation is supplied through a loud speaker attached to the bottom of the suspension container. b) Schematics of the azimuth-dependent transmission measurements. The incident and azimuth angles with respect to the [111] axis are denoted by θ and φ, respectively. The inset shows the unfolded first Brillouin zone of a fcc lattice, showing the high symmetry points. The dotted line along the $L'KLUX$ orientations corresponds to a sample rotation by varying θ at $\varphi = 0°$ and the dashed circle represents the trace of the incident light beam by varying the angle φ at $\theta = 65°$.

ADVANCED FUNCTIONAL MATERIALS

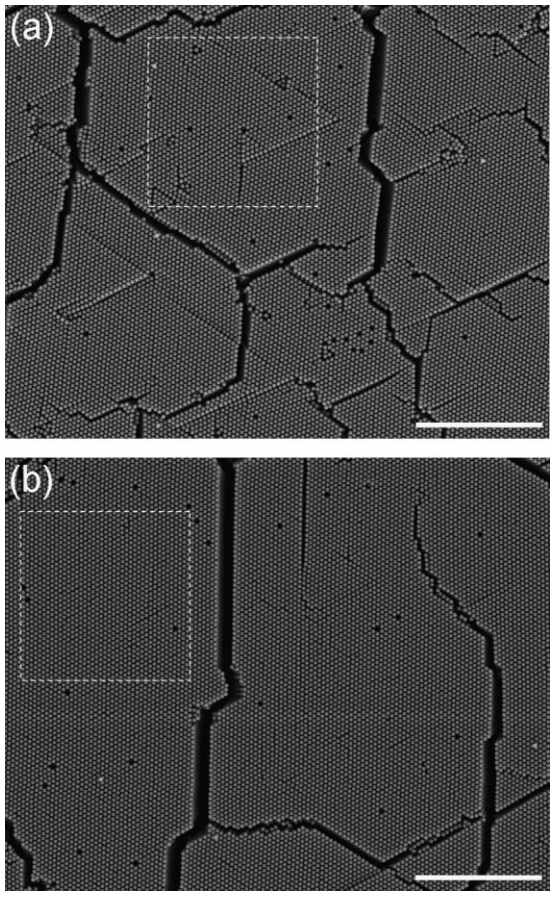

Figure 2. SEM images of the opal films A (a) and B (b) opal films. The white bar denotes 10 μm.

3. Ordering of Spheres in the (111) Growth Plane

Figure 2 shows the SEM images of the A and B opal films. The images were captured with the same magnification, brightness, and contrast along the film normal. Comparing images one can conclude that the sample B grown in the acoustic field has ordered crystallites with transverse dimensions lager than those of the sample A grown without noise agitation. The cracks separating the crystallites appear due to the release of the stress accumulated in the lattice due to shrinkage of spheres in the dried crystal. The random configuration of cracks in sample A corresponds to the randomness of the lattice deformation during the evaporation of the water. The preferential alignment of cracks along the drawing direction indicates a more ordered lattice crystallized under the acoustic agitation. A thorough statistical analysis of noise-dependent regularity of the opal lattice[34] demonstrated the need of a specific vibration magnitude for an optimum crystalline quality.

The opals ordering is usually estimated from SEM images of the uppermost (111) plane, namely, the hexagonal 2-D lattice of spheres oriented parallel to the substrate. FT patterns of the SEM images in Figure 2 are presented in Figure 3. These patterns were obtained from the whole imaged areas including cracks (Fig. 3a and b) and from small crack-free areas indicated by the white rectangles (Fig. 3c and d).

The FT pattern of an ideal infinitely large lattice should contain only harmonics of the lattice period. In reality, the FT patterns consist of the points, crosses, lines, diffuse rings, and the background. The points in Figure 3a–d represent harmonics of the periodic structure in the SEM image. In practice, the randomness of the real lattice dissolves this pattern. The ratio of the background brightness to the intensity at diffraction spots characterizes the resolution of harmonics. The resolution depends, in the first place, on the number of elements in the analyzed ensemble. If this number decreases, a brighter background is observed. The stronger background in Figure 3c and d as compared to Figure 3a and b is due to smaller sampled area. Consequently, in a correct comparison, the lattice images should contain the same number of unit cells. Diffuse rings appear due to azimuth misalignment of the lattices in crystallites. They are more pronounced in Figure 3a and b, but appear to be about the same for both samples. The white crosses around the points in the FT pattern are the consequence of a limited number of spheres in the images. Such edge effect is more pronounced in patterns corresponding to small lattice areas. The lines connecting points are the frequency components, which satisfy the lattice symmetry, but appear irregularly in the images. They are more pronounced in the center of Figure 3a and c than in Figure 3b and d. This observation corroborates the positive role of noise upon crystallographic ordering in the (111) plane.

Which of these features characterize the lattice perfection in the most straightforward way? For a perfect lattice composed of sharp bright spots, which can be approximated by an array of delta functions, $p(x)$, composed of m elements separated in space by an interval T, $p(x) = \sum_{m=-\infty}^{\infty} \delta(x - mT)$. The corresponding FT harmonics are all of the same magnitudes described by $P(f) = \frac{1}{T} \sum_{n=-\infty}^{\infty} \delta(f - mT_f)$, where $T_f = 1/T$. In contrast, the magnitude of the harmonic in a disordered lattice decreases with the harmonic index. Therefore, the ratio of the harmonic magnitudes quantifies the identity and the spatial resolution of the lattice points in the SEM image. The uniformity of the lattice spacing across the image corresponds to the magnitude of the first harmonic. Thus, by comparing the magnitudes of the first harmonic of different FT patterns one can judge which lattice is more ordered.

The ordering of the two lattices in Figure 2a and b was estimated in accordance with the above guidelines and the results are shown in Figure 3e and f. In order to avoid the contribution from the edge effect, the magnitudes of the harmonics in the FT power spectrum were traced along the diagonals shown by the white dashed lines in the figures and then averaged to reduce random fluctuations. It is seen that the powers (M) of all the FT harmonics are higher for the sample B, indicating a better regularity of its lattice. In the FT pattern of the large lattice areas (Figure 3e), the noise agitation causes the

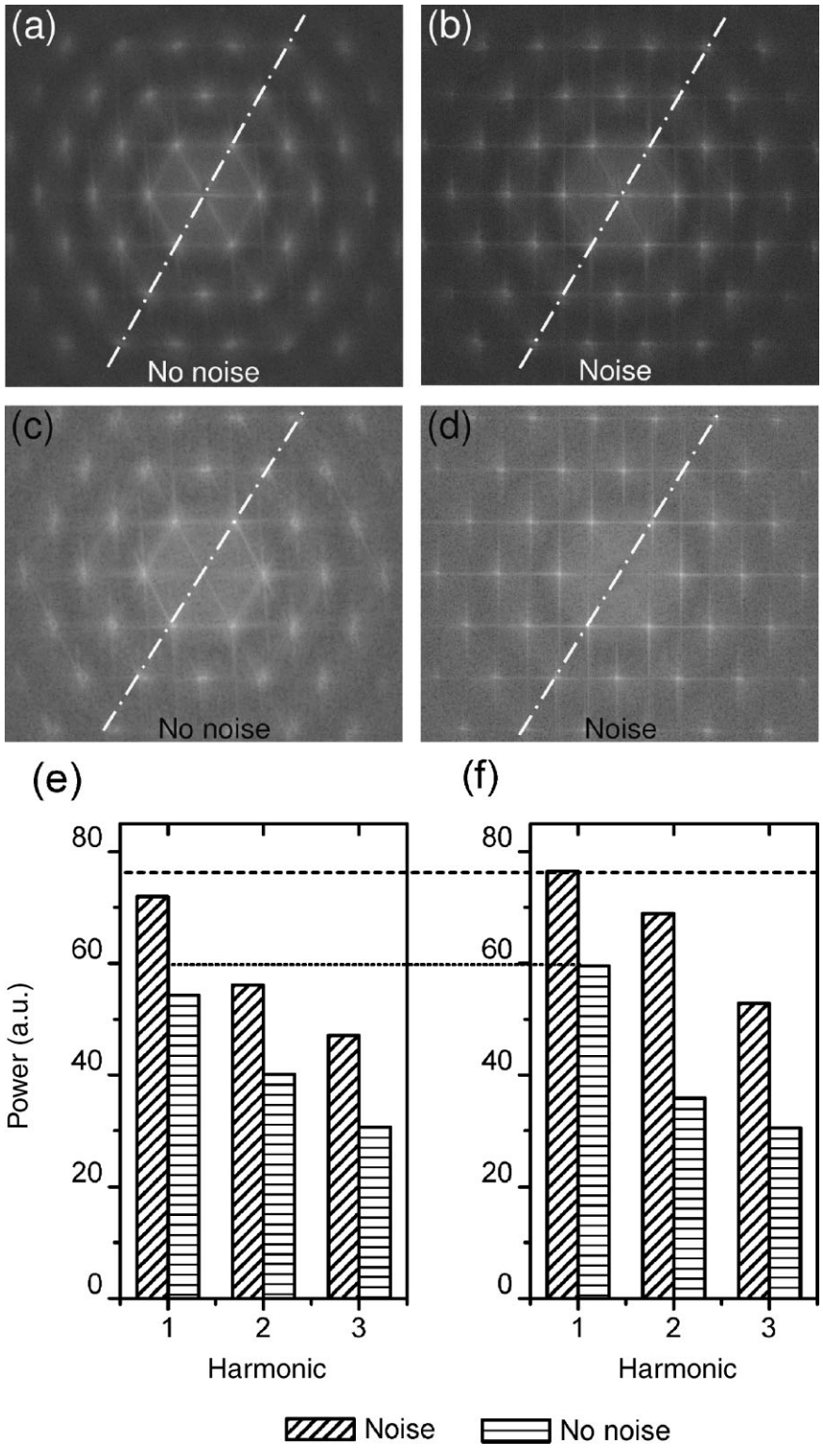

Figure 3. FT patterns of the SEM images in Figure 2 obtained from a), b) whole areas of these images and c), d) from the areas circumscribed by the white rectangles in Figure 2. The panel e) and f) show the magnitudes of the first three harmonics in the FT patterns shown in panels a and b, and panels d and e, respectively.

same increase in the magnitudes of all the harmonics, $\Delta M = 16$. This means that, on average, the noise agitation results in a 30% improvement of the sphere lattice ordering in the (111) plane. If the effect of opal cracks is excluded from the analysis, the magnitudes of the 1st harmonic increase by less than 5% for both samples.

On the other hand, the distribution of the magnitudes of higher harmonics differs dramatically if the crack-free area is inspected. In particular, the difference between samples A and B is $\Delta M = 17$, 33, and 22 for the first, the second, and the third harmonics, respectively, indicating the higher lattice ordering in the crystallites of film B. The apparently lower decrease rate of harmonic magnitudes for the B sample points to a lower concentration of lattice defects in this sample. For example, the ratio M_1/M_2 reduces from 1.7 in the A sample to 1.1 in the B sample (Figure 3f). This clearly corresponds to the improved sharpness and symmetry of lattice points in the SEM image of the sample B.

Results of the FT analysis of SEM images are limited to the resolution of the data file and to the sampled area, i.e., this approach remains a local one. Nevertheless, it provides guidelines for experimental work on optimization of crystallization conditions.

4. Transmission as a Function of the Light Incidence Angle

Nowadays, the commonly accepted spectroscopy evidence of opal lattice order is the observation of the structure-related resonances in the transmittance/reflectance spectra in the range of reduced frequencies $a/\lambda \leq 1.8$, where $a = \sqrt{2}D$ is the constant of the fcc lattice.[35] Less common is the understanding that all these features, except the resonance, which occurs at the longest wavelengths, do not belong to the photonic bandgaps but to the diffraction at crystal planes.[36,37] Thus, the examination of the angular dispersion of these resonances against the Bragg law can be used to assess the conformity of the opal lattice to the fcc lattice symmetry.

Transmission spectra obtained at the angles (θ, φ) of (0,0), (65,0), and (65,50)

ADVANCED FUNCTIONAL MATERIALS

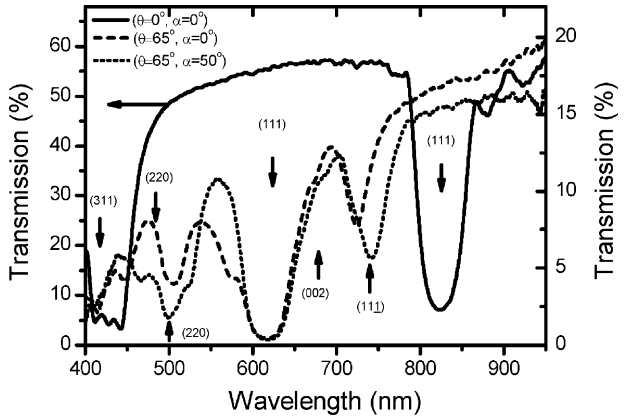

Figure 4. Transmission spectra of the sample B at $\theta = 0°, \varphi = 0°$ (solid curve), oblique incidence $\theta = 65°, \varphi = 0°$ (dashed curve), and $\theta = 65°, \varphi = 50°$ (dotted curve). Arrows are labeled according to crystal planes providing the diffraction attenuation.

are shown in Figure 4 to introduce the studied diffraction resonances from different lattice planes in the reduced frequency range from 0.52 to 1.3. The transmission spectrum of opal film is rich with minima; moreover, the position of these minima changes with angle of the light incidence and with the rotation of the incidence plane. We set a criterion of 3% attenuation and the traceability of these minima in the range $-70° \leq \theta \leq 70°$ of the angles of incidence to discriminate them from the background noise.

By plotting the central wavelength of the transmission minimum as a function of the incidence angle, θ, the dispersion curve $\lambda_0(\theta)$ can be obtained (Fig. 5, open circles). In order to facilitate the discussion, the dispersion branches are labeled with *xi* symbols, where *x* corresponds to the panel letter from a to f and *i* represents the number of the branch. For example, *a*1 means branch 1 in the panel a. The dispersions of diffraction resonances expected in the fcc lattice according to the Bragg law are shown by lines. Details of the fitting procedure are given in Section 7.

Experimentally observed dispersions for three azimuth directions of opal films A and B are compared to the Bragg resonance dispersions expected in the fcc lattice with the same lattice parameter, as shown in Figure 5. Let us consider the dispersion of resonances according to increase in the crystallography indices of corresponding planes.

(1) (111) planes: In agreement with common practice, a perfect fitting is achieved for the (111) diffraction resonance dispersion across the whole angle range except in the directions of the multiple wave diffraction,[38] namely, for $\theta = \pm(45 - 55°)$. The sphere diameter $D = 368$ nm and the effective index of refraction $n_{\text{eff}} = 1.37$ were extracted from this fit.

(2) (020) and $(11\bar{1})$ planes: The most striking feature is observation of a mixture of (020) and $(11\bar{1})$ diffraction resonances since none of them follows exactly the dispersion for the fcc lattice. In a perfect fcc lattice, scanning along the LK direction probes diffraction at $\{11\bar{1}\}$ while scanning along the LU direction probes the (020) resonances.[39] Scanning along the LW direction can bring both resonances together in the one spectrum (inset to Fig. 1b). In contrast, both (020) and $(11\bar{1})$ resonances (a2 and a1, respectively) are seen along the LK line on the surface of the fcc Brillouin zone for the sample A (Fig. 5a), whereas only the $(11\bar{1})$ resonance is observed for sample B (d2) (Fig. 5d). Along the LU line, only the $(11\bar{1})$ is observed in sample A (Fig. 5c) instead of the expected (020) resonance, whereas both resonances can be observed in sample B (Fig. 5f). Along the LW line both (020) and $(11\bar{1})$ resonances are present (b1, b2, e1, and e2) but their appearance is more regular in the sample B (Fig. 5e). Fitting these dispersions to the Bragg law suggests an increase in the inter-plane distances for $(11\bar{1})$ and (020) sets of planes by 4.2 and 2.4%, respectively. This increase is accompanied by a corresponding increase in the inter-plane angle, leading to the opposite shift of these resonances along the LW line by 2.2 and 2.4%, respectively. This distortion of the opal lattice is, provisionally, the reason for the observed mixture of diffraction resonances along the directions where otherwise only one resonance is expected. This observation supports the suggested stretching of the opal lattice in samples grown in a vertically moving meniscus.[37] In agreement with the SEM inspection of these samples, the analysis of the diffraction resonance dispersions also suggest that the acoustic noise agitation allows a close-to-equilibrium conditions for opal crystallization in a moving meniscus and leads to opal lattice approaching the fcc symmetry. In spite of this distortion, we will retain the notation for the fcc lattice in the subsequent discussion.

(3) (220) Plane: A good correlation between fcc lattice resonances and experimental data are observed for the (220) diffraction branch, denoted as the branch 6. However, in this spectral range, the branch (4) and the tripled (220) resonance branches (5 and 7) in the LK panel differ quite significantly from the diffraction in the fcc lattice. For example, the tripling of the (220) branch translates into an increase and a decrease in the original (220) inter-plane spacing by 4.4 and 7.6%, respectively. Since the [220] axis is directed along the (111) plane, these deviations are caused provisionally by the lattice stretching associated with changes of $(11\bar{1})$ and (020) plane spacings.

(4) Short wavelengths range: $\lambda < 450$nm. None of the diffraction branches 8–11 can be unambiguously assigned to that at the fcc lattice planes, because the opal lattice distortion gives rise to strong changes in the inter-plane distances and to new lattice planes. Moreover, at small angles of incidence (8) the light attenuation by diffraction resonances in the 3-D lattice is accompanied

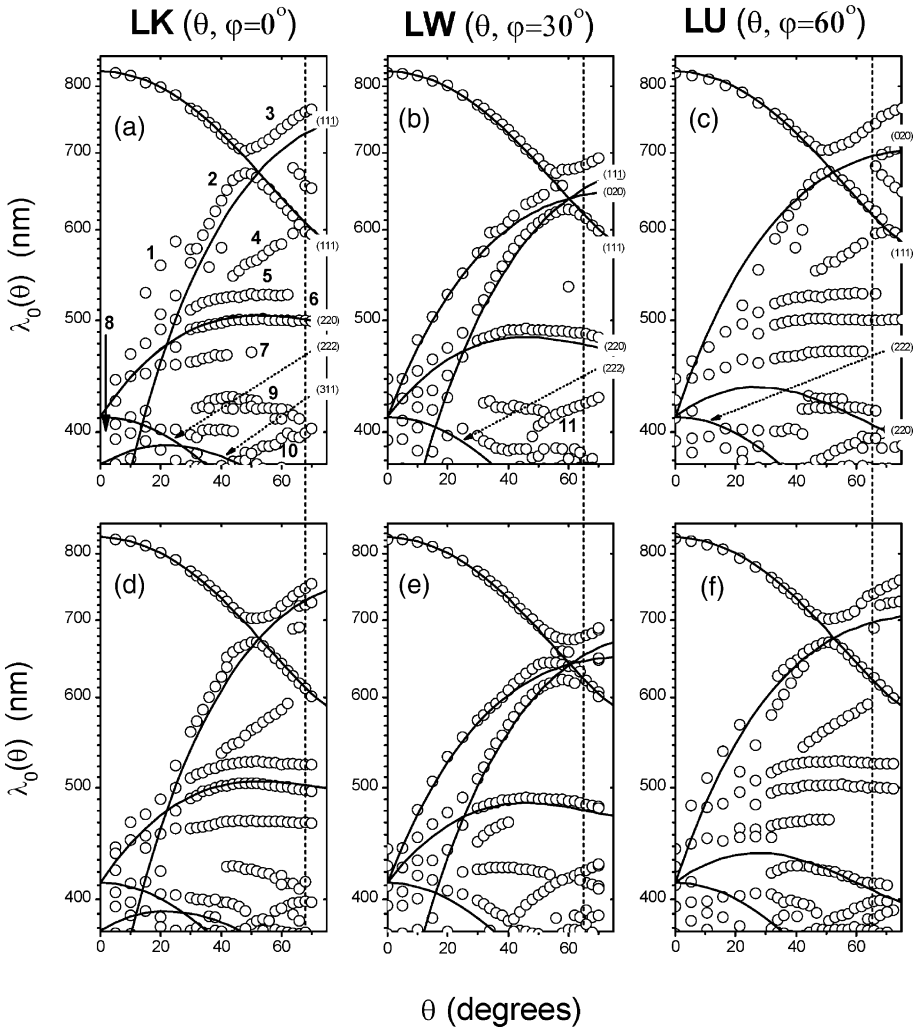

Figure 5. Dispersion of transmission minima as a function of the incident angle (θ) along *LK*, *LW*, and *LU* lines on the surface of the Brillouin zone, as indicated, for the samples A a), b), c) and B d), e), f) opal films. Lines labeled with (*hkl*) indices of crystal planes show the expected dispersion of diffraction resonances in the fcc lattice.

by losses to the excitation of 2-D evanescent modes which propagates along the film surface.[40]

These observations point to the general character of the lattice deviation from the fcc symmetry occurring in opals crystallized in a moving meniscus and show that the acoustic noise agitation makes opal lattice more ordered within one and the same generic configuration. It is worth noting that, the similarity in $\lambda_0(\theta)$ curves between the *LK* and *LU* line, but not along the *LW* line suggests twinning of the lattice in the studied samples.[17–19] The construction of a self-consistent picture of the distorted opal lattice symmetry remains beyond the scope of this paper, since it requires extensive numerical modeling.

In the context of the present work, we conclude that the traditional analysis of the diffraction resonance dispersions fails to provide a self-contained quantitative measure of the lattice ordering if ordering is to be quantified by the deviation from an independently introduced standard. For opals the latter is, usually, the Bragg diffraction in the fcc lattice or the numerically calculated PBG structure of the corresponding PhC, which is too general a choice in the case of a stretched lattice.[41]

5. Transmission as a Function of the Lattice Orientation

The overall trigonal symmetry is ascribed to the fcc lattice. Having evidence that the actual symmetry of the lattice in the opal films crystallized in the moving meniscus differs from the fcc one, it becomes vitally important to examine its rotational symmetry by turning the plane of incidence around the [111] axis. The fact that transmission changes with the azimuth angle is apparent from the comparison of the dotted and dashed spectra in Figure 4. In order to improve the visibility of fine details, the transmission data were transformed into extinction data, i.e., $-\log(T)$. Extinction spectra obtained from transmission data measured at $\theta = 65^\circ$ are presented in contour plots as a function of the azimuth angle of the plane of incidence and the wavelength for the samples crystallized with and without noise agitation (Fig. 6a and b). The meaning of this plot is to demonstrate how similar is the diffraction attenuation provided by crystal planes belonging to the same family. The principle justification for such examination is the assumption of the direct correlation between the regularity of the extinction pattern and the lattice periodicity.

The higher regularity of the extinction pattern is apparent for the sample B (Fig. 6b), but it would be instructive to represent this impression quantitatively. This was achieved by applying the FT analysis to the extinction diagram at fixed wavelengths.

Figure 7a and b compare contributions of the 180, 60, and 30° periodic features in extinction diagrams (Fig. 6a and b) through the FT power spectrum at different wavelengths. The corresponding harmonics demonstrate the superposition of the 2-, 6-, and 12-fold axial symmetry in the azimuth transmission pattern. The particular wavelengths are chosen to highlight the effect of the lattice ordering and reveal the crystal planes,

ADVANCED FUNCTIONAL MATERIALS

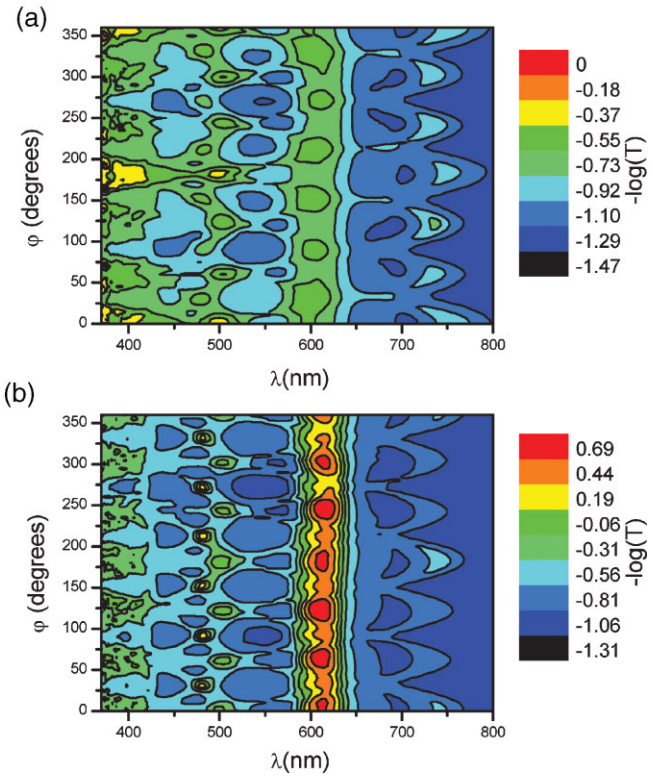

Figure 6. Contour plots of the extinction surface as a function of wavelength (λ) and azimuth angle (φ) for the incident angle of $\theta = 65°$ for A (a) and B (b) samples.

which are the most vulnerable to the opal lattice disorder. Data in Figure 7 demonstrate that the dominating periodicity is the six-fold axial symmetry. Generally, this periodicity is superimposed on two other symmetries.

At $370 \leq \lambda \leq 400$ nm, the six-fold symmetry dominates the patterns of both samples, whereas for the sample A a significant contribution from the two-fold symmetry is present. Pure six-fold axial symmetry is observed at $\lambda = 400$ nm for both samples and the magnitudes of the corresponding harmonic are the same. In this spectral range the diffraction at (311) planes should appear only in LUK orientation producing a three-fold rotational symmetry. Observation of the three-fold symmetry is, apparently, the consequence of stacking faults in the opal lattice (Fig. 5).

In the range $450 \leq \lambda < 500$ nm both samples retain six-fold symmetry. The two-fold symmetry dominates the pattern of the sample A, while it is absent in that of the sample B. In addition, the 12-fold axial symmetry is also present in the extinction pattern, the corresponding harmonic of which dominates the power spectrum at $\lambda = 480$ nm for both samples. It is noteworthy that in the sample B the magnitudes of the 6- and 12-fold harmonics are 10-times higher than the corresponding values in the sample A. In this spectral range the major attenuation is provided by diffraction resonance at planes related to (220) planes of the fcc lattice. At $\lambda = 510$ nm, the six-fold symmetry prevails in both samples, for which the corresponding harmonic is two times stronger in the pattern of the sample B. The 6-fold symmetry dominates up to $\lambda \leq 540$ nm, but it is accompanied by 12-fold harmonic for both samples. The difference is that the sample A possesses an additional two-fold symmetry. In this wavelength range the diffraction is also provided by planes related to (220) family of fcc lattice.

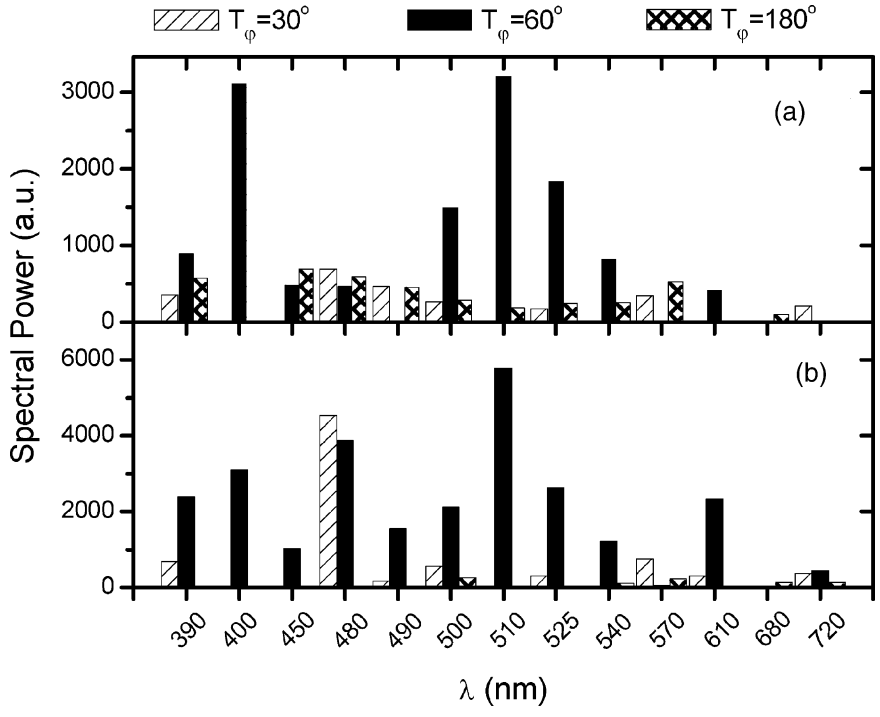

Figure 7. The three Fourier components $T_\varphi = 30$, 60, and 180° of the FT power spectra obtained from $-\log T(\varphi)$ curves at different wavelengths for the opal films A (a) and B (b).

At $\lambda = 570$ nm, no six-fold symmetry was registered for both samples. Instead they show 12-fold symmetry and a persisting 2-fold pattern dominating the extinction in the sample A. This pattern cannot be associated with diffraction in the fcc lattice.

At longer wavelengths the transmission is dominated by the strong (111)diffraction resonance centered at 610 nm, the azimuth pattern of which complies with the six-fold symmetry. The corresponding harmonic in the sample B is about five times higher than in the sample A. In the wavelength range of diffraction at (020) and $(11\bar{1})$ planes the extinction pattern looks disordered, which is reflected by the mixture of harmonics with small magnitudes.

On average, the analysis of the extinction pattern shows that the opal

B is approximately two times more ordered than the opal film A. The susceptibility of the crystal ordering to non-equilibrium conditions of the lattice crystallization is not the same for all crystal planes. The most pronounced, up to ten times difference, is related to the formation of (220) planes. It is noteworthy that this is the direction along all (111) planes but the growth plane. The magnitude of the corresponding 6-and 12-fold harmonics can be suggested to act as a benchmark to compare samples of different crystalline qualities.

In order to generalize the azimuth-dependent spectroscopy approach, similar data were analyzed for the transmission at another angle of incidence, namely $\theta = 30°$. The overall picture remains the same, whereas some effects of noise agitation on lattice ordering are less pronounced.

In summary, it is worth emphasizing that FT analysis of azimuth extinction diagrams is based on the repetition of similar features provided by crystal planes of the same family. This makes the suggested analysis of the colloidal crystal ordering a self-contained quantitative method operating independently on the type of the lattice symmetry.

6. Conclusions

We quantified the difference in crystal ordering of two opal films assembled with and without acoustic agitation using the FT analysis of the SEM images and optical diffraction experiments.

The ordering of spheres in the (111) lattice of the growth plane was characterized using the magnitudes of harmonics in the FT pattern of the SEM images. A quantitative comparison of different samples becomes possible assuming the same brightness and contrast of the images and taking into account the areas containing an equal number of the lattice unit cells in the inspected portion of the lattice. We compared the magnitude of the 1st harmonic in FT pattern to estimate the regularity of the sphere spacing, and the decrease rate of the magnitudes of higher harmonics to evaluate the sharpness of the ordering resolution of the spheres. The 30% improvement in the in-plane lattice ordering was assigned to the effect of acoustic noise upon the crystallization of the opal films. It is worth noting that cracks in the opal film do not affect strongly the lattice spacing, but lead to a decrease in magnitude of the higher harmonics in the FT pattern.

The dispersion of diffraction minima in the angle-resolved transmission spectra demonstrates unambiguously the strong deviation of the opal lattice from the fcc symmetry. The lattice distortion includes changing the inter-plane distances and angles that leads to the appearance of additional lattice planes. The 4% stretching of the opal lattice perpendicular to the drawing direction was estimated and provisionally assigned to the directionality of opal crystallization in a moving meniscus. Softening the spheres anchoring conditions on the substrates by chaotic displacement of spheres due to acoustic agitation improves the lattice ordering but does not change the lattice symmetry.

A quantitative assessment of the ordering of lattice planes in a 3-D crystal was achieved employing the optical transmission spectroscopy as a function of the rotation angle of the plane of light incidence with respect to the crystal lattice. The FT pattern of the extinction obtained as a function of the azimuth angle reveals the superposition of 2-, 6-, and 12-fold rotation axes. We found that the composition of these harmonics in the FT pattern changes with the wavelength in correspondence to changing the crystal planes dominating the diffraction. This allows us to characterize the rotational symmetry and the regularity of these planes in the lattice. It is observed that the diffraction at (220) planes is the most sensitive to the disorder, showing about ten-time ordering improvement for opal crystallized in the noise acoustic field. Overall, approximately two-time better ordering of high-index lattice planes is assigned to the opal film crystallized with the aid of acoustic noise vibration.

Finally, we should emphasize the generic form of the FT analysis to the evaluation of opal crystal ordering based on repetitive features observed in the SEM images and in the axial extinction diagrams. This approach offers convenient and effective complimentary quantitative methods of the analysis of in-plane and three-dimensional lattice ordering of three-dimensional PhC.

7. Experimental

The PMMA spheres were synthesized with a median diameter (D) = 368 nm using the modified surfactant-free emulsion polymerization technique [42]. The PMMA spheres were then dispersed in deionized water with a resistivity of 18 MΩ-cm to obtain the desired concentration 4 wt %. The opal films were self-crystallized on glass substrates, which were vertically drawn out of the suspension by a stepping motor at an approximate speed of 1.5 mm hr^{-1}. The acoustic vibration in the form of the white noise with a frequency band spanning from 20 to 4000 Hz, was applied during the growth process through a loudspeaker attached to the bottom of the suspension container. Figure 8 shows the frequency spectrum of the white noise. The crystallization process was carried out at room temperature under controlled relative humidity of $32 \pm 2\%$.

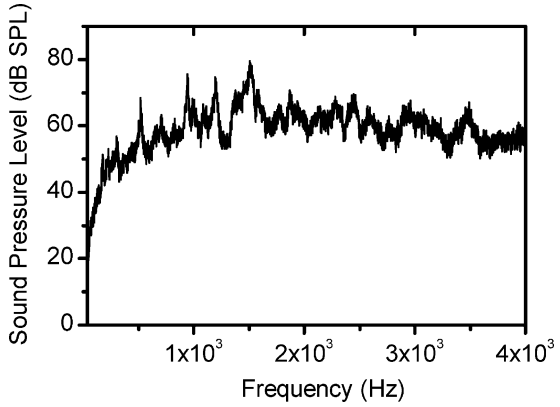

Figure 8. Power spectral density of the white noise.

ADVANCED FUNCTIONAL MATERIALS

The SEM images were captured with Carl Zeiss field emission SEM (FESEM) SUPRA™ 40. The corresponding FT patterns were obtained by the two-dimensional Discrete FT (DFT) technique:

$$F(u,v) = \sum_{x=0}^{M-1}\sum_{y=0}^{N-1} f(x,y)\exp\left(\frac{-i2\pi}{M}ux\right)\exp\left(\frac{-i2\pi}{N}vy\right) \quad (1)$$

where $f(x,y)$ represents the spatial domain function and $F(u,v)$ is the corresponding FT.

Angle-resolved transmission measurements were performed to trace the dispersion of diffraction resonances in the opal films. Samples were mounted on a two-axis rotation stage, which allows to change to the angle of incidence, θ and, simultaneously, to rotate the plane of the light incidence with respect to the lattice by changing the azimuth angle, φ. The white light from a halogen lamp, shaped as a parallel beam with a diameter of ca. 1 mm using an optical telescope, was directed to the samples. The transmitted light was collected from a solid angle of approximately 3° to allow the angle-resolved measurement and detected by a broadband high-resolution CCD spectrometer.

The dispersions of the diffraction resonance wavelengths $\lambda_o(\theta)$ for different planes of the opal lattice were compared with the Bragg law predictions for the fcc lattice:

$$\lambda = 2n_{\text{eff}}d_{hkl}\sqrt{(1-\sin^2(\alpha_{hkl})} \quad (2)$$

where d_{hkl} is the inter-planar distance of the (hkl) planes, n_{eff} the effective index of refraction, and α_{hkl} is the angle between the incident light and the normal vector to the (hkl) lattice planes. The $n_{\text{eff}} = 1.37$ and $D = 368$ nm were obtained as fitting parameters from the Bragg fit to the experimental dispersion of the diffraction resonance at the (111) growth planes.

The power spectrum of the extinction pattern was calculated using one-dimensional DFT, and only those harmonics with power more than 10% of the peak power are shown.

Received: December 6, 2007
Revised: March 10, 2008
Published online: July 23, 2008

[1] J. D. Joannopoulos, R. D. Meade, J. N. Winn, *Photonic Crystals: Molding the Flow of Light*, Princeton University Press, Singapore **1996**.
[2] S. G. Johnson, P. Villeneuve, S. Fan, J. D. Joannopoulos, *Phys. Rev. B* **2000**, *62*, 8212.
[3] O. Painter, R. K. Lee, A. Scherer, A. Yariv, J. D. O'Brien, P. D. Dapkus, I. Kim, *Science* **1999**, *284*, 1819.
[4] M. Qiu, B. Jaskorzynska, *Appl. Phys. Lett.* **2003**, *83*, 1074.
[5] M. Bayindir, B. Temelkuran, E. Ozbay, *Appl. Phys. Lett.* **2000**, *77*, 3902.
[6] M. Imada, S. Noda, A. Chutinan, T. Tokuda, M. Murata, G. Sasaki, *Appl. Phys. Lett.* **1999**, *75*, 316.
[7] D. A. Mazurenko, R. Kerst, J. I. Dijkhuis, A. V. Akimov, V. G. Golubev, D. A. Kurdyukov, A. B. Pevtsov, A. V. Sel'kin, *Phys. Rev. Lett.* **2003**, *91*, 213903.
[8] M. Scharrer, A. Yamilov, X. Wu, H. Cao, R. P. H. Chang, *Appl. Phys. Lett.* **2006**, *88*, 201103.
[9] K. Busch, S. John, *Phys. Rev. E* **1998**, *58*, 3896.
[10] S. Noda, N. Yamamoto, A. Sasaki, *Jpn. J. Appl. Phys.* **1996**, *35*, L909.
[11] M. Campbell, D. N. Sharp, M. T. Harrison, R. G. Denning, A. J. Turberfield, *Nature* **2000**, *404*, 53.
[12] I. Divliansky, T. S. Mayer, K. S. Holliday, V. H. Crespi, *Appl. Phys. Lett.* **2003**, *82*, 1667.
[13] S. Y. Lin, J. G. Fleming, D. L. Hetherington, B. K. Smith, R. Biswas, K. M. Ho, M. M. Sigalas, W. Zubrzycki, S. R. Kurtz, J. Bur, *Nature* **1998**, *394*, 251.
[14] K. Aoki, H. T. Miyazaki, H. Hirayama, K. Inoshita, T. Baba, K. Sakoda, N. Shinya, Y. Aoyagi, *Nature* **2003**, *2*, 117.
[15] P. Jiang, J. F. Bertone, K. S. Hwang, V. L. Colvin, *Chem. Mater.* **1999**, *11*, 2132.
[16] L. V. Woodcock, *Nature* **1997**, *385*, 141.
[17] Y. A. Vlasov, V. N. Astratov, A. V. Baryshev, A. A. Kaplyanskii, O. Z. Karimov, M. F. Limonov, *Phys. Rev. E* **2000**, *61*, 5784.
[18] R. M. Amos, J. G. Rarity, P. R. Tapster, T. J. Shepherd, *Phys. Rev. E* **2000**, *61*, 2929.
[19] S. A. Asher, J. M. Weissman, A. Tikhonov, R. D. Coalson, R. Kesavamorthy, *Phys. Rev. E* **2004**, *69*, 66619.
[20] L. Cademartiri, A. Sutti, G. Calestani, *Langmuir* **2003**, *19*, 7944.
[21] Y. A. Vlasov, X. Z. Bo, J. C. Strum, D. J. Norris, *Nature* **2001**, *414*, 289.
[22] Y. W. Chung, I. C. Leu, J. H. Lee, M. H. Hon, *Langmuir* **2006**, *22*, 6454.
[23] S. H. Park, D. Qin, Y. Xia, *Adv. Mater.* **1998**, *10*, 1028.
[24] B. Griesebock, M. Egen, R. Zentel, *Chem. Mater.* **2002**, *14*, 4023.
[25] H. Miguez, F. Meseguer, C. Lopez, A. Mifsud, J. S. Moya, L. Vazquez, *Langmuir* **1997**, *13*, 6009.
[26] Y. H. Ye, F. LeBlanc, A. Hache, V. V. Truong, *Appl. Phys. Lett.* **2001**, *78*, 52.
[27] S. Wong, V. Kitaev, G. A. Ozin, *J. Am. Chem. Soc.* **2003**, *125*, 15589.
[28] H. Fudouzi, *J. Colloid Interface Sci.* **2004**, *275*, 277.
[29] E. Palacios-Lidón, B. H. Juárez, E. Castillo-Martínez, C. López, *J. Appl. Phys.* **2005**, *97*, 63520.
[30] a) H. Graetsch, K. Ibel, *Phys. Chem. Miner.* **1997**, *24*, 102. b) I. M. Sosnowska, M. Shiojiri, *J. Electron Microsc.* **1999**, *48*(6), 681.
[31] a) M. Megens, C. M. van Kats, P. Bösecke, W. L. Vos, *Langmuir* **1997**, *13*, 6120. b) W. L. Vos, M. Megens, C. M. van Kats, P. Bösecke, *Langmuir* **1997**, *13*, 6004.
[32] F. García-Santamaría, J. F. Galisteo-López, P. V. Braun, C. López, *Phys. Rev. B* **2005**, *71*, 195112.
[33] J. Huang, N. Eradat, M. E. Raikh, Z. V. Vardeny, A. A. Zakhidov, R. H. Baughman, *Phys. Rev. Lett.* **2001**, *86*, 4815.
[34] W. Khunsin, A. Amann, G. Kocher, S. G. Romanov, E. P. O'Reilly, C. M. Sotomayor Torres, in preparation.
[35] J. F. Galisteo-López, C. López, *Phys. Rev. B* **2005**, *70*, 35108.
[36] E. Pavarini, L. C. Andreani, C. Soci, M. Galli, F. Marabelli, D. Comoretto, *Phys. Rev. B* **2005**, *72*, 45102.
[37] S. G. Romanov, *Phys. Solid State* **2007**, *49*(3), 536.
[38] S. G. Romanov, T. Maka, C. M. Sotomayor Torres, M. Müller, R. Zentel, D. Cassagne, J. Manzanares-Martinez, C. Jouanin, *Phys. Rev. E* **2001**, *63*, 56603.
[39] J. F. Galisteo-Lopez, E. Palacios-Lidon, E. Castillo-Martinez, C. Lopez, *Phys. Rev. B* **2003**, *68*, 115109.
[40] S. G. Romanov, M. Bardosova, M. Pemble, C.M Sotomayor Torres,, *Appl. Phys. Lett.* **2006**, *89*, 043105.
[41] V. Babin, P. Garstecki, R. Holyst, *Appl. Phys. Lett.* **2003**, *82*, 1553.
[42] M. Mueller, R. Zentel, T. Maka, S. G. Romanov, C. M. Sotomayor Torres, *Chem. Mater.* **2000**, *12*, 2508.

